An Impedance-Based Stability Analysis Method for Paralleled Voltage Source Converters

Wang, Xiongfei; Blaabjerg, Frede; Loh, Poh Chiang

Published in:
Proceedings of the 2014 International Power Electronics Conference (IPEC-Hiroshima 2014 - ECCE-Asia)

DOI (link to publication from Publisher):
10.1109/IPEC.2014.6869788

Publication date:
2014

Document Version
Early version, also known as pre-print

An Impedance-Based Stability Analysis Method for Paralleled Voltage Source Converters

Xiongfei Wang, Frede Blaabjerg, and Poh Chiang Loh
Department of Energy Technology, Aalborg University, Aalborg, Denmark
xwa@et.aau.dk, fbl@et.aau.dk, pcl@et.aau.dk

***Abstract*— This paper analyses the stability of paralleled voltage source converters in AC distributed power systems. An impedance-based stability analysis method is presented based on the Nyquist criterion for multiloop system. Instead of deriving the impedance ratio as usual, the system stability is assessed based on a series of Nyquist diagrams drawn for the terminal impedance of each converter. Thus, the effect of the right half-plane zeros of terminal impedances in the derivation of impedance ratio for paralleled source-source converters is avoided. The interaction between the terminal impedance of converter and the passive network can also be predicted by the Nyquist diagrams. This method is applied to evaluate the current and voltage controller interactions of converters in both grid-connected and islanded operations. Simulations and experimental results verify the effectiveness of theoretical analysis.**

Keywords*— *Impedance-based analysis, Nyquist criterion, paralleled voltage source converters, stability

I. INTRODUCTION

Voltage source converters have commonly been found in renewable energy generation systems, energy-efficient drives, and high-performance electronics equipment. The interactions of the paralleled or cascaded voltage source converters are challenging the stability and power quality in AC distributed power systems [1]. The constant power operation of these converters may destabilize the system with low-frequency oscillations [2]. The inner current or voltage control loops of converters may also interact with each other, and with the resonance conditions brought by the output *LCL* or *LC* filters and parasitic capacitances of power cables, resulting in resonances in a wide frequency range [3]. There is, consequently, an increasing research concern over the interaction of interconnected converters.

The impedance-based analytical approach has widely been used for the stability analysis of power-electronics-based power systems [4]-[8]. The minor-loop gain, which is defined as the terminal impedance ratio of the source and load converters, is proved to be effective to analyze the interactions of interconnected converters [4]. Several stability criteria have been derived based on the minor-loop gain, including the Gain Margin and Phase Margin (GMPM) criterion [5], the opposing argument criterion [6], the Energy Source Analysis Consortium (ESAC) criterion [7], and the maximum peak criterion [8]. The different forbidden regions are thus defined to derive the impedance specification of the load converter for a given source converter impedance. All of the impedance-based stability criteria assume that the minor-loop gain has no Right Half-Plane (RHP) poles [8]. This is justified in the source-load converter systems, since each converter is designed with a stable terminal behavior. However, in the multiple paralleled source-source converter systems, such as wind farms, photovoltaic power plants, and paralleled uninterruptible power supplies, this prerequisite imposes the constraint on the derivation of impedance ratio. The presence of RHP zeros in the converter impedance may induce the RHP poles in the minor-loop gain [9]-[10].

To mitigate the influence of RHP zeros, two stability criteria have been recently reported, i.e. the passivity-based stability criterion [9], and the impedance sum type criterion [10]. The passivity-based stability criterion is derived from the frequency-domain passivity theory [11], which has been used earlier for current controller design of voltage source converters [12]. Generally, the passivity of the converter impedance is defined that the impedance has no RHP poles and has a positive real part. The system is stable if all the converter impedances are passive. Thus, the derivation of impedance ratio is avoided. This method allows the robust design of controllers for converters, yet is still a sufficient stability condition, since the negative real part of impedance does not indicate the instability of system. In contrast, the impedance sum type criterion is directly based on the characteristic equation of the minor feedback loop, which is the sum of converter impedances [10]. The encirclement of the origin in the complex plane indicates the instability of system. This criterion provides a sufficient and necessary stability condition and works well in the paralleled source-source converter systems. However, by this means, it is difficult to characterize the contribution of each converter to the stability in a system with multiple paralleled converters.

To reveal how the paralleled source-source converters interact with each other and with the passive components, this paper presents an impedance-based stability analysis method by means of the Nyquist criterion for multiloop systems. Instead of deriving the impedance ratio, a series of Nyquist diagrams drawn for the converter impedances and passive components are adopted to predict the system stability. Thus, the effect of RHP zeros in the converter

This work was supported by European Research Council (ERC) under the European Union's Seventh Framework Program (FP/2007-2013)/ERC Grant Agreement n. [321149-Harmony].

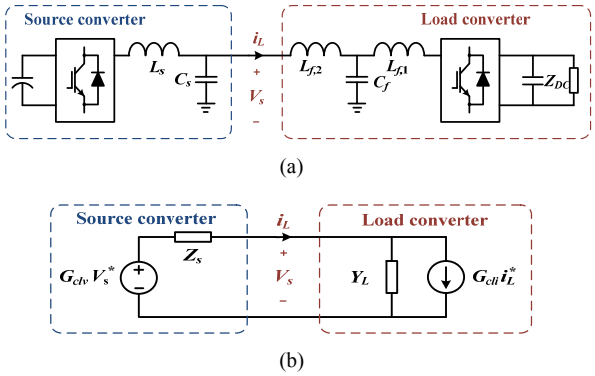

Fig. 1. A cascaded source-load converter system and equivalent circuit. (a) Basic configuration. (b) Equivalent circuit.

impedances can be avoided. This approach is applied to evaluate the current and voltage controller interactions of converters in both grid-connected and islanded operations. Simulations and experiments verify the effectiveness of theoretical analysis.

II. Impedance-Based Stability Criterion

A. Source-Load Converter System

Fig. 1 shows a typical cascaded source-load converter system and the equivalent circuit to illustrate the basic principle of the impedance-based stability criterion. The closed-loop response of the source converter voltage and the load converter current can be given by

$$i_L(s)=\underbrace{\frac{1}{1+Z_sY_L}}_{\text{Minor loop}}\left[G_{cli}i_L^*+Y_LG_{clv}V_s^*\right] \tag{1}$$

$$V_s(s)=\underbrace{\frac{1}{1+Z_sY_L}}_{\text{Minor loop}}\left[G_{clv}V_s^*-Z_sG_{cli}i_L^*\right] \tag{2}$$

where G_{cli} and Y_L denote the current reference-to-output transfer function and closed-loop input admittance of the load converter, respectively. G_{clv} and Z_s are the voltage reference-to-output transfer function and the closed-loop output impedance of the source converter, respectively. If the converters are designed with stable terminal behavior, i.e. G_{cli} and G_{clv} have no RHP poles, the overall system stability will be merely dependent on the minor feedback loop composed by the impedance product, Z_sY_L, which is also termed as the minor-loop gain.

In this scenario, due to the stable terminal behaviors of converters, the minor-loop gain has no RHP poles and the encirclement of the point (-1, j0) indicates the instability of the system.

B. Source-Source Converter System

Fig. 2 illustrates a paralleled source-source converter system operating in grid-connected and islanded modes. Similarly, the impedance-based model of this system can be derived based on the terminal behaviors of converters, which is shown in Fig. 3. The converters are represented

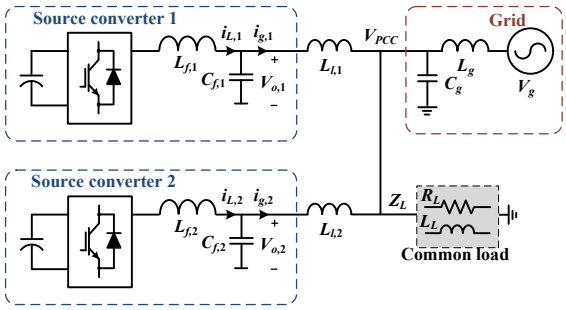

Fig. 2. A paralleled source-source converters system operating in grid-connected and islanded modes.

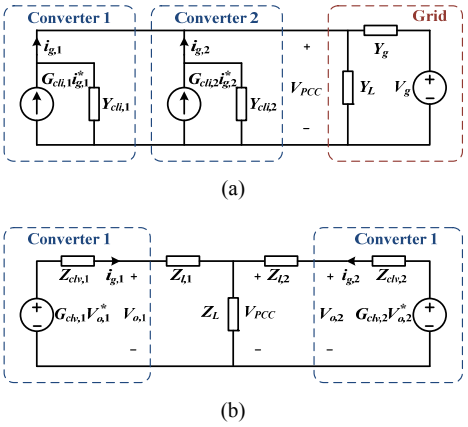

Fig. 3. Impedance-based equivalent circuit of paralleled source-source converter system in (a) grid-connected mode and (b) islanded mode.

by the Norton equivalent circuits in the grid-connected mode and the Thevenin equivalent circuits in the islanded mode. Thus, the closed-loop responses of the converters output currents and voltages in grid-connected mode and islanded mode, as well as the Point of Common Coupling (PCC) voltage can be derived in the following

$$i_{g,k}=\frac{G_{cli,k}i_{g,k}^*}{1+Y_{cli,k}/Y_{toi,k}}-\frac{Y_{cli,k}/Y_{toi,k}}{1+Y_{cli,k}/Y_{toi,k}}\left(G_{cli,j}i_{g,j}^*+Y_gV_g\right) \tag{3}$$

$$Y_{toi,k}=Y_{cli,j}+Y_g\quad\begin{cases}k,\ j\in\{1,2\}\\ k\neq j\end{cases} \tag{4}$$

$$V_{PCC}=\frac{1}{1+Y_{cli,k}/Y_{toi,k}}\cdot\frac{G_{cli,k}i_{g,k}^*+G_{cli,j}i_{g,j}^*+Y_gV_g}{Y_{toi,k}} \tag{5}$$

$$V_{o,k}=\frac{G_{clv,k}V_{o,k}^*}{1+Z_{clv,k}/Z_{tov,k}}-\frac{Z_{clv,k}/Z_{tov,k}}{1+Z_{clv,k}/Z_{tov,k}}G_{clv,j}V_{o,j}^* \tag{6}$$

$$Z_{tov,k}=Z_{clv,j}+Z_{l,j}+Z_{l,k} \tag{7}$$

$$i_{g,k}=\frac{1}{1+Z_{clv,k}/Z_{tov,k}}\cdot\frac{G_{clv,k}V_{o,k}^*-G_{clv,j}V_{o,j}^*}{Z_{tov,k}} \tag{8}$$

where $G_{cli,k}$ and $G_{cli,j}$ are the current reference-to-output transfer functions. $Y_{cli,k}$ and $Y_{cli,j}$ denote the closed-loop

output admittances of converters in grid-connected mode. $G_{clv,k}$ and $G_{clv,j}$ are the voltage reference-to-output transfer functions, and $Z_{clv,k}$ and $Z_{clv,j}$ are the closed-loop output impedances of converters in the islanded operation. The effect of load, Y_L and Z_L, is disregarded. $Z_{tov,k}$ and $Y_{toi,k}$ are the equivalent system impedance and admittance of the k-th converter seen from the PCC, respectively.

Following (1) and (2), the minor-loop gain for the k-th converter in the grid-connected and islanded modes can be represented by the impedance ratios of $Y_{cli,k}/Y_{toi,k}$ and $Z_{clv,k}/Z_{tov,k}$, respectively. However, unlike the source-load converter systems, the equivalent system impedance may have RHP zeros due to the effect of passive components and the j-th converter. Consequently, the minor-loop gain will have RHP poles, and the system may be stable even if the Nyquist diagram encircles the point (-1, j0). Hence, the stability criteria derived for the cascaded source-load converter system may not be applicable for the paralleled source-source converter system.

C. Presence of RHP Zeros

Fig. 4 shows the control block diagrams of converters in the grid-connected and islanded operations. Tables I and II list the parameters of electrical constants and the controllers which are used in this study.

Since the current and voltage controller interactions of converters are concerned in this work, the power control and grid synchronization loops are neglected. The single-loop grid current control is adopted in the grid-connected mode for the inherent active damping of *LCL* resonance [13], and the double-loop voltage control scheme is used in the islanded mode. The Proportional Resonant (PR) controller is used for control the grid current and output voltage with zero steady-state error.

Fig. 5 gives a comparison on the pole-zero maps of the system equivalent impedance and the terminal impedance of converter. It is clear that the RHP zeros present in the system impedance and admittance, yet no RHP zeros can be observed in the converter impedance and admittance. This implies that even if the terminal impedances has no RHP zeros, the interaction of the converters impedances and passive components may bring the RHP zeros into the system impedances. It is noted that the presence of RHP zeros implies that the impedance has the negative real part. However, the negative real part of impedance does not necessarily indicate the presence of RHP zeros.

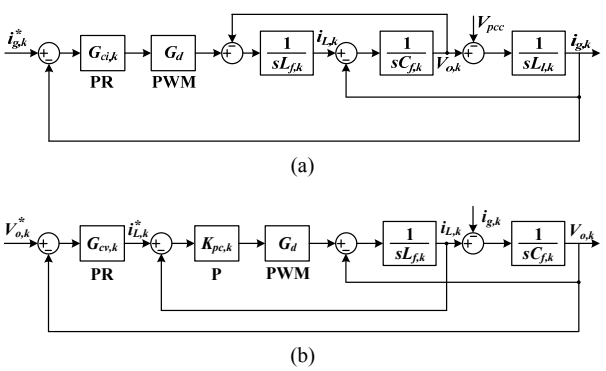

Fig. 4. Block diagrams of (a) the current control loop in grid-connected mode, and (b) the voltage control loop in the islanded mode.

TABLE I
ELECTRICAL PARAMETERS

Symbol	Meaning	Value
V_g	Line-line grid voltage	400 V
f_1	Grid frequency	50 Hz
L_g	Grid inductance	1.5 mH
C_g	Grid capacitance	2 μF
$L_{f,k}$	Filter inductor	1.8 mH
$C_{f,k}$	Filter capacitor	10 μF
$L_{l,k}$	Line inductance	0.9 mH
f_{sw}	Switching frequency	10 kHz
$V_{dc,k}$	DC-link voltage	750 V
R_L	Load resistance	80 Ω
L_L	Load inductance	166 mH

TABLE II
CONTROLLER PARAMETERS

Symbol	Meaning	Value
$K_{pg,k}$	Proportional gain of PR grid current controller	8
$K_{ig,k}$	Integral gain of PR grid current controller	500
$K_{pv,k}$	Proportional gain of PR voltage controller	0.005
$K_{iv,k}$	Integral gain of PR voltage controller	200
$K_{pc,k}$	Proportional converter current controller	8
T_s	Sampling period	100 μs

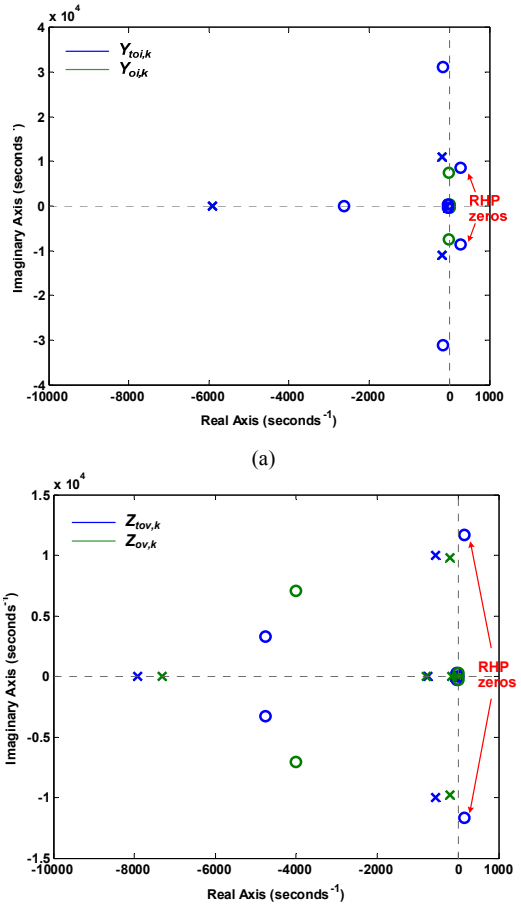

Fig. 5. Pole-zero maps of the (a) system equivalent admittance $Y_{toi,k}$ (zoom on origin) and (b) system impedance $Z_{tov,k}$ (zoom on origin).

III. PROPOSED ANALYSIS METHOD

This section reviews the Nyquist stability criterion for multiloop systems, and then presents an impedance-based stability analysis method to address the influence of RHP zeros in the conventional impedance ratio type criteria.

A. Nyquist Criterion for Multiloop Systems

The Nyquist criterion was generalized to the multiloop systems by Bode [14], which may be stated as follows:

"A linear multiloop system is stable if and only if the total numbers of clockwise and counterclockwise encirclements of the point (-1, *j*0) are equal to each other in the series of Nyquist diagrams drawn for the individual loops obtained by beginning with all loops open and closing the loops successively in any order to their normal configuration [15]."

From Fig. 3, it can be seen that the impedance-based equivalent model of the interconnected converter system is basically a multiloop system. Thus, instead of deriving the overall open-loop gain of the minor feedback loop, the system stability can also be predicted by the series of Nyquist diagrams of the individual loops according to the Nyquist criterion for multiloop systems. Consequently, the effect of the RHP zeros in the system impedance can be avoided.

B. Stability Analysis of Source-Source Converter System

Fig. 6 illustrates a block diagram representation of the impedance-based equivalent circuit in Fig. 3. The minor feedback loop for the *k*-th converter is decomposed into two local loops by converter impedances. The stability of the minor feedback loop is thus assessed by successively closing the two loops and analyzing the Nyquist diagrams drawn for them. The system is stable if the total numbers of clockwise and counterclockwise encirclements of the point (-1, *j*0) are equal to each other in these Nyquist diagrams. Moreover, by this means, how each converter contributes to the system stability can be revealed by the Nyquist diagrams of local loops.

Fig. 7 shows the Nyquist diagrams of two loops in the grid-connected operation. First, the loop that is composed by the grid impedance and the *j*-th converter admittance, $T_{ik,1}$ is evaluated, and then the loop including the *k*-th converter admittance, $T_{ik,2}$ is assessed.

$$T_{ik,1}(s)=\frac{Y_{cli,j}}{Y_g} \quad \Rightarrow \quad T_{ik,2}(s)=\frac{Y_{cli,k}}{Y_g+Y_{cli,j}} \tag{9}$$

It is seen that only the Nyquist diagram of $T_{ik,1}$ encircles the point (-1, *j*0) once in the clockwise direction, which indicates that the system is unstable. Further, the Nyquist diagram of $T_{ik,1}$ also implies that the interaction between the *j*-th converter and grid impedance leads to instability when the *k*-th converter is disconnected. Thus, to attain a stable system, the *k*-th converter impedance should make the minor feedback loop encircle the point (-1, *j*0) once in counterclockwise direction. As a consequence, the design specification for the converter admittance can be derived from the Nyquist diagrams of local loops.

Fig. 8 shows the Nyquist diagrams of two loops in the islanded operation, in which the loop gains are given by

$$T_{vk,1}(s)=\frac{Z_{clv,j}}{Z_{l,k}+Z_{l,j}} \quad \Rightarrow \quad T_{ik,2}(s)=\frac{Z_{cli,k}}{Z_{l,k}+Z_{l,j}+Z_{clv,j}} \tag{10}$$

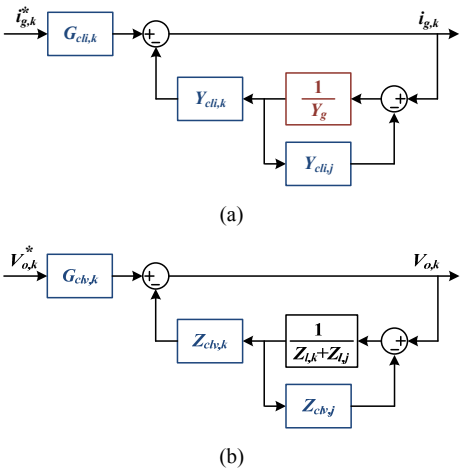

Fig. 6. Block diagram of the impedance-based equivalent system model. (a) Grid-connected mode. (b) Islanded mode.

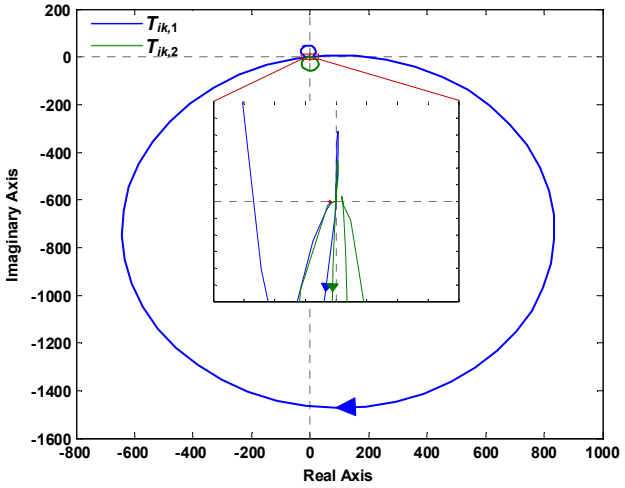

Fig. 7. Nyquist diagrams of two loops in the grid-connected operation.

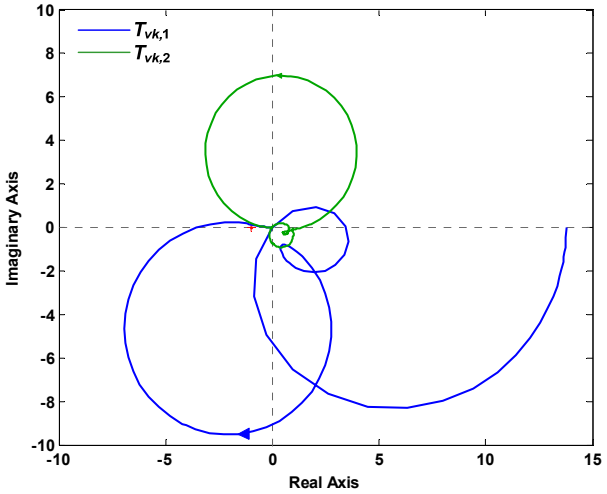

Fig. 8. Nyquist diagrams of two loops in the islanded operation.

Similarly to Fig. 7, the local feedback loop including the *j*-th converter impedance and line impedances is first assessed, and then the minor feedback loop with the *k*-th converter impedance is analyzed with Nyquist diagrams. It is seen that only the Nyquist diagram of $T_{vk,1}$ encircles the point (-1, *j*0), which implies that the overall system is unstable. Further, the Nyquist diagram of $T_{vk,1}$ shows that the interaction of the *j*-th converter and line impedances cause instability when the *k*-th converter is disconnected. Therefore, to stabilize the islanded operation with the *k*-th converter, the terminal impedance $Z_{clv,k}$ should be shaped so that the Nyquist diagrams of two loops have the same numbers of clockwise and counterclockwise encirclement of the point (-1, *j*0)

Fig. 9 shows the control diagram for the *k*-th converter to shape the output impedance $Z_{clv,k}$. A feedback of the output voltage of the *k*-th converter is employed in the filter current control loop. In contrast, the control scheme

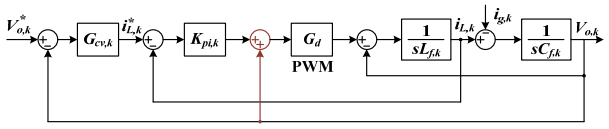

Fig. 9. Block diagram of the *k*-th converter in the islanded operation with the output voltage feedback in the filter current control loop.

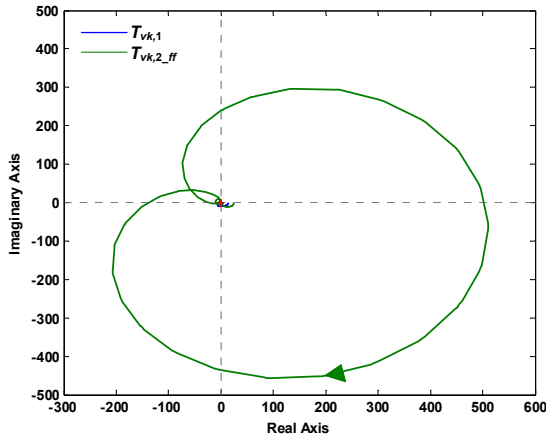

(a)

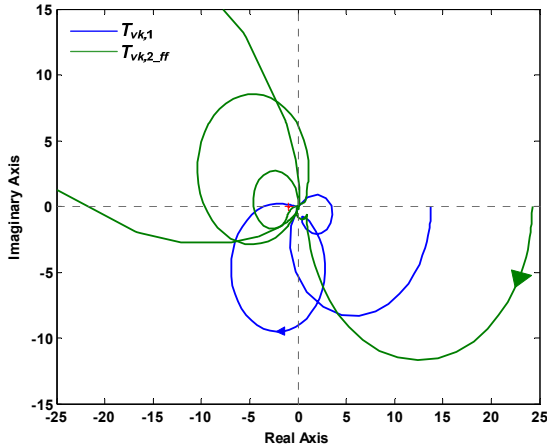

(b)

Fig. 10. Nyquist diagrams of two loops in the islanded operation with the modified control diagram for the *k*-th converter. (a) Full view. (b) Zoomed out around (-1, *j*0).

for the *j*-th converter keeps the same as Fig. 4 (b). Fig. 10 shows the Nyquist diagrams of two loops. The loop $T_{vk,1}$ is the same as Fig. 8, while the loop $T_{vk,2}$ has encircles the point (-1, *j*0) once in the clockwise and twice in the counterclockwise directions. As a consequence, the total numbers of clockwise and counterclockwise encirclement of the point (-1, *j*0) are equal to each other. The islanded operation of the system is stable.

It is worth noting that this stability analysis approach can also be generalized to the *N*-paralleled source-source converter systems. The minor feedback loop for a given source converter can be divided into the *N* local feedback loops, which include *N*-1 loops to model the effect of the other $N-1$ paralleled source converters, and the minor feedback loop. Thus, how the source converters interact with each other and with the passive components can be successively assessed by the series of Nyquist diagrams drawn for the *N* loops.

IV. Simulations and Experimental Results

To validate the theoretical analyses, the time-domain simulations using PLECS Blockset and MATLAB, and the experimental tests based on two Danfoss frequency converters are carried out. The converters are powered by the constant DC voltage sources. The control algorithms in experiments are implemented in the DS1006 dSPACE system, in which the DS2004 high-speed Analog/Digital board is used for the sampling and the DS5101 waveform generation board is used for the Pulse Width Modulation (PWM) pulses generation.

A. Grid-Connected Operation

Fig. 11 shows the simulated grid currents of converters and the PCC voltage in the grid-connected operation. The unstable oscillations can be observed, which confirms the stability analysis in Fig. 7. However, due to the presence of RHP zeros in the equivalent system impedance, if only the admittance ratio $Y_{cli,k}/Y_{toi,k}$ is evaluated by the Nyquist diagram, then the instability cannot predicted.

Fig. 12 shows the measured grid currents and the PCC voltage waveforms in the grid-connected operation. It can

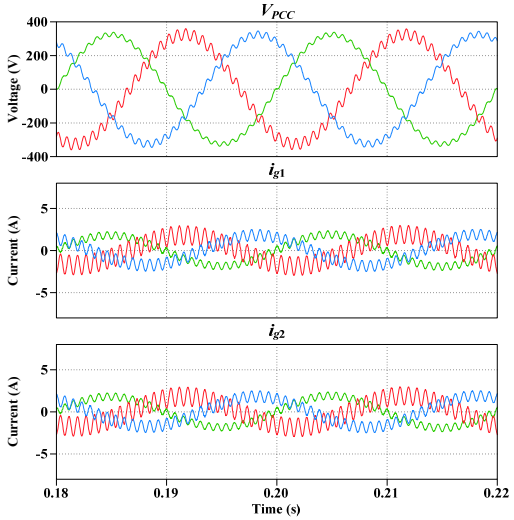

Fig. 11. Simulated grid currents of converters and the PCC voltage in grid-connected operation.

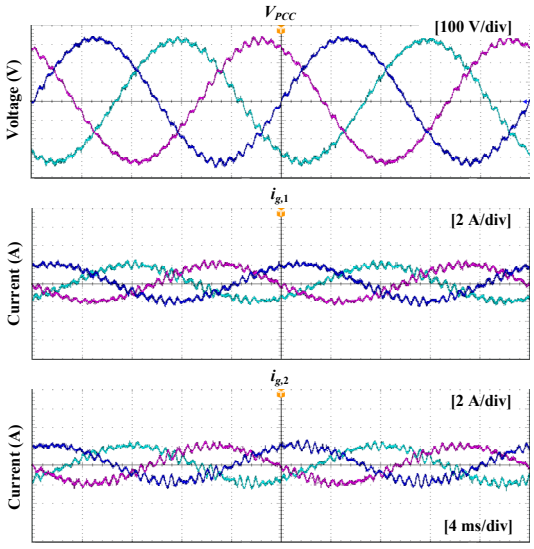

Fig. 12. Measure grid currents of converters and the PCC voltage in the grid-connected operation.

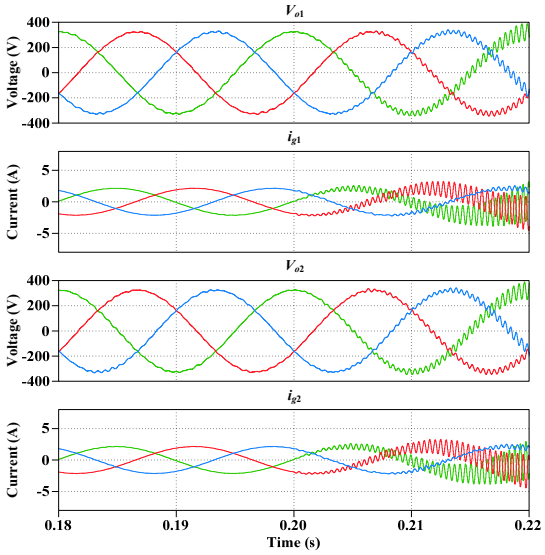

Fig. 13. Simulated converters output voltages and currents based on the control scheme in Fig. 4 (b).

be seen that the experimental tests matches well with the simulation results, which also again verify the theoretical analysis with the Nyquist criterion for multiloop systems.

B. Islanded Operation

Two simulation case studies are carried out to evaluate the system stability in the islanded operation, in order to validate the theoretical analyses shown in Figs. 8 and 10.

Fig. 13 shows the simulated converters output voltages and currents based on the control scheme shown in Fig. 4 (b). The converters are connected in parallel at the time instant of 0.2 s. It is clear that both of the converters are stable when operating standalone, and becomes unstable when they are connected together. This implies that the stable terminal behaviors of converters are designed. The interactions of converters with each other and with the line inductances result in the system instability, which verifies the stability analysis in Fig. 8. Similarly, if only

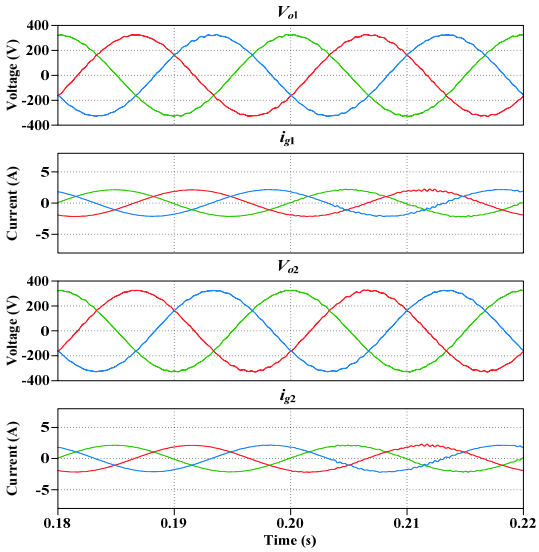

Fig. 14. Simulated converters output voltages and currents based on the control scheme in Fig. 4 (b).

the Nyquist diagram of the impedance ratio $Z_{clv,k}/Z_{tov,k}$ is assessed following the conventional stability criteria, the opposite conclusion will be drawn.

Fig. 14 shows the simulated waveforms when one of the converters adopts the control scheme shown in Fig. 9. A stable system operation can be observed even when the two converters are connected in parallel. This agrees with the analysis in Fig. 10, and confirms the Nyquist criterion for multiloop systems when there are multiple clockwise and counterclockwise encirclements of the point (-1, j0).

V. Conclusions

This paper has discussed the stability analysis for the paralleled source-source converter systems. The effect of the RHP zeros in deriving the minor-loop gains of source converters has been analyzed. It has been shown that the equivalent system impedance may have the RHP zeros, due to the interaction of converter impedance and passive components. To reveal how each converter interacts with each other and with passive components, an impedance-based stability analysis approach has been proposed with the Nyquist stability criterion for multiloop systems. The effect of RHP zeros is avoided in this method. Simulation and experimental case studies validate the effectiveness of the theoretical analyses.

References

[1] J. Sun, "Small-signal methods for AC distributed power systems–a review," *IEEE Trans. Power Electron.*, vol. 24, pp. 2545-2554, Nov., 2009.

[2] T. Messo, J. Jokipii, J. Puukko, and T. Suntio, "Determining the value of DC-link capacitance to ensure stable operation of a three-phase photovoltaic inverter," *IEEE Trans. Power Electron.*, vol. 29, no. 2, pp. 665-673, Feb. 2014.

[3] X. Wang. F. Blaabjerg, M. Liserre, Z. Chen, J. He, and Y. W. Li, "An active damper for stabilizing power-electronics-based AC systems," *IEEE Trans. Power Electron.*, vol. 29, no. 7, pp. 3318-3329, Jul. 2014.

[4] R. D. Middlebrook, "Input filter design considerations in design and applications of switching regulators," in *Proc. IEEE IAS* 1976, pp. 366-382.

[5] C. M. Wildrick, F. C. Lee, B. H. Cho, and B. Choi, "A method of defining the load impedance specification for a stable distributed power system," *IEEE Trans. Power Electron.*, vol.10, no. 3, pp. 280-285, May 1995.

[6] X. Feng, J. Liu, F. C. Lee, "Impedance specifications for stable DC distributed power systems," *IEEE Trans. Power Electron.*, vol.17, no. 2, pp. 157-162, Mar. 2002.

[7] S. D. Sudhoff, S. F. Glover, P. T. Lamm, D. H. Schmucker, and D. E. Delisle, "Admittance space stability analysis of power electronic systems," *IEEE Trans. Aero. & Electron.*, vol. 36, no. 3, pp. 965-973, Jul. 2000.

[8] S. Vesti, T. Suntio, J. A. Oliver, R. Prieto, and J. A. Cobos, "Impedance-based stability and transient-performance assessment applying maximum peak criteria," *IEEE Trans. Power Electron.*, vol.28, no. 5, pp. 2099-2104, May 2013.

[9] A. Riccobono and E. Santi, "A novel passivity-based stability criterion (PBSC) for switching converter DC distribution systems," in *Proc. IEEE APEC* 2012, pp. 2560-2567.

[10] F. Liu, J. Liu, H. Zhang, and D. Xue, "Stability issues of Z+Z type cascade system in hybrid energy storage system (HESS)," *IEEE Trans. Power Electron.*, in press, 2014.

[11] J. C. Willems, "Dissipative dynamical systems Part I: general theory," *Arch. Ration. Mech. Anal.*, vol. 45, pp. 321-351, 1972.

[12] L. Harnefors, L. Zhang, and M. Bongiorno, "Frequency-domain passivity-based current controller design," *IET Power Electron.*, vol. 1, no. 4, pp. 455-465, Dec. 2008.

[13] J. Yin, S. Duan, and B. Liu, "Stability analysis of grid-connected inverter with LCL filter adopting a digital single-loop controller with inherent damping characteristic" *IEEE Trans. Ind. Inform*., vol. 9, no. 2, pp. 1104-1112, May 2013.

[14] H. W. Bode, *Network analysis and feedback amplifier design*, Van Nostrand, New York, 1945.

[15] B. J. Lurie and P. J. Enright, *Classical feedback control with MATLAB® and Simulink®*, Boca Raton, FL, CRC Press, Taylor & Francis Group, 2011.